X CONGRESSO NACIONAL DE ENGENHARIA MECÂNICA 2018
ABCM
20 A 24 DE MAIO DE 2018 SALVADOR – BA – BRASIL

TRAJECTORIES ESTIMATION NEAR A BINARY ASTEROID

J. B. Silva Neto, jose.batista@inpe.br[1]
H. K. Kuga, helio.kuga@inpe.br[2]
A. F. B. A. Prado, antonio.prado@inpe.br[1]

[1]National Institute for Space Research - INPE, Av. dos Astronautas, 1.758 - Jardim da Granja, São José dos Campos - SP, 12227-010
[2]Technological Institute of Aeronautics - ITA, Praça Marechal Eduardo Gomes, 50 - Vila das Acacias, São José dos Campos - SP, 12228-900

Abstract: *The interest in asteroids has increased in recent years, with several missions underway or in the planning phase. Considering the technological challenges for navigation around such small bodies, often dealing with multiple systems, such as the asteroid binary system 65803 Didymos (1996 GT), our study analyzed the use of the Extended Kalman Filter in minimizing position errors and velocity in the navigation of a spacecraft in a binary system of astetoids. After the development of the filter for a generic double system, a case study was made for the asteroid binary system Didymos 65803 (1996 GT), including the analysis of the naming filter error of position and speed of observations of the Moon's orbit called Didymoon. At the end of the study, we can conclude that the Extended Kalman filter showed a good behavior in minimizing position and velocity errors of the spacecraft and Didymoon.*
Keywords: *Asteroid, spacecraft navigation, Extended Kalman filter.*

1. INTRODUCTION

The study of asteroids represents an important step in understanding the formation of our solar system. Another important motivation for developing missions for asteroids, is the risk of colliding asteroids with Earth. A more recent motivation lies in the commercial exploration of asteroids through mining. With these motivations several missions are underway or being planned to study them.

The study and exploration of asteroids represent a great technological challenge, much is under development and there are several problems to be solved. One of the challenges that will be the focus of the present study is the navigation around these small bodies, often multiple systems, where bodies are often very close. As an example we have the asteroid 65803 Didymos (1996 GT), which has a moon (Didymoon) orbiting the main body (Didymos), target of the mission Asteroid Impact & Deflection Assessment (AIDA) (Michel *et al.*, 2016). Nowadays, in deep-space navigation missions, star sensors, planetary sensors, pulsars, doppler effect, among other methods, are used to determine the position and velocity of a spacecraft in deep space (Jagannathan, 1994; Wood *et al.*, 2012; Rad and Azari, 2014). However, when it comes to asteroids with such tiny dimensions, new solutions that make navigation as autonomous and accurate as possible have been developed. One of the more modern methods, called autonomous optical navigation, uses the spacecraft's own camera to determine its position and velocity (Riedel *et al.*, 2000; Cui and Zhu, 2014).

Knowing the challenges involved in determining the orbits of spacecraft in asteroid environments, the present study will analyze the use of the extended Kalman filter as a means of minimizing errors from the position and velocity sensor measurements of an orbiting spacecraft of a double asteroid.

The study was developed as follows:

- Since this is a nonlinear system, the extended Kalman filter was used;
- The filter was developed for a dual generic system, with a primary body at the center of the inertial frame and a secondary one in orbit around the primary. The direct and indirect perturbations of the secondary body of the system on the movement of the spacecraft were considered;
- A complete model was developed, which was numerically integrated. This model will provide the reference measures; White noise was added to the reference measurements from the complete model. These averages were used as sensor measurements in the update phase of the extended Kalman Filter; The asteroid Didymos was chosen as the target of a deeper analysis of the extended Kalman filter;
- The behavior of the filter and the impact of the estimation for the Didymoon trajectory and of a spacecraft navigating in the Didymos-Didymoon system were analyzed.

2. METHODS

2.1 Full Model

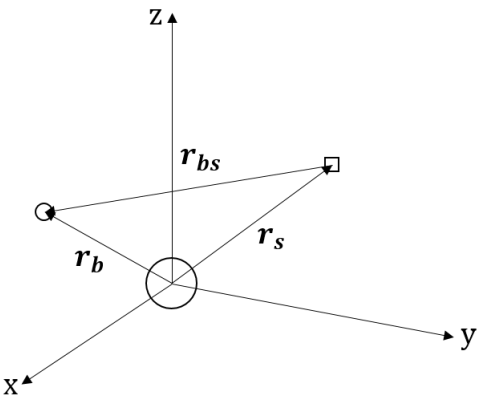

Figura 1: Representation of the binary system.

Consider the system shown in Figure 1, where a spacecraft orbits a system consisting of a main body (Alpha) and a moon orbiting this body (Beta). This spacecraft will be subject to the gravitational forces of Alpha and Beta, as well as the non-sphericity of the main body. The model also considers the solar radiation pressure and the gravitational forces of the bodies in the vicinity. It is considered eccentric orbits for the asteroids because this is the most common situation. It is also considered the perturbation caused by Earth, Jupiter, Mars and Venus. It will also be considered the effect of non-sphericity of the bodies Alpha and Beta. Thus, the equations of motion for Beta and for the spacecraft, relative to the inertial frame positioned at the center of Alpha, are given, respectively, by:

$$\ddot{\mathbf{r}}_b = -\frac{\mu_{ab}}{r_b^3}\mathbf{r_b} + \mathbf{P}_{shape,b} \tag{1}$$

where $\mu_{ab} = G\left(m_a + m_b\right)$, being G the universal gravitational constant, m_a the mass of Alpha and m_b the mass of Beta. $\mathbf{r}_b$ is the position vector of the Beta and $\mathbf{P}_{shape,b}$ is the acceleration due to non-sphericity of Alpha in the Beta motion.

$$\ddot{\mathbf{r}}_s = -\frac{\mu_a}{r_s^3}\mathbf{r_s} + \mu_b\left[\frac{\left(\mathbf{r_b}-\mathbf{r_s}\right)}{\left(r_b - r_s\right)^3} - \frac{\mathbf{r_b}}{r_b^3}\right] + \mathbf{P}_{shape,s} + \mathbf{P}_{SRP} + \mathbf{P}_{3C} \tag{2}$$

where $\mu_a = Gm_a$ and $\mu_b = Gm_b$ and $\mathbf{r}_s$ is the position vector of the spacecraft. $\mathbf{P}_{shape,s}$ is the acceleration due to non-sphericity of Alfa in the spacecraft motion. $\mathbf{P}_{SRP}$ is the acceleration due to solar radiation pressure. $\mathbf{P}_{3C}$ is the sum of the accelerations due to all the planets considered and Didymoon. The second term of Equation 2 refers to the third disorder caused by Beta, where the direct and indirect disturbances are considered.

2.2 Extended Kalman Filter

The extended Kalman filter is applied to nonlinear systems. The present study considered the model of non-linear and linear measurements, where the measurements are provided in a linear manner directly by the simulated sensor. The measures (y) come directly from the real model presented in Section 2.1 where a white noise (zero mean noise) was inserted into these measurements. In this way, we have:

$$\dot{\mathbf{x}} = \mathbf{f}\left(\mathbf{x}\right) \tag{3}$$

$$\mathbf{y_k} = \mathbf{H}\mathbf{x} + \boldsymbol{\nu_k} \tag{4}$$

where x are the states, $\mathbf{f}$ is the non-linear vector function of the state $\mathbf{x}$ in the time t, $\boldsymbol{\nu}$ is the white noise and $\mathbf{H}$ is the matrix that relates the measurements to the parameters. Through the expansion of $\mathbf{f}$ in Taylor series and truncating to the linear term, we arrive at (Kuga, 2005):

$$\mathbf{F} = \begin{bmatrix} \frac{\partial f_1(\mathbf{X})}{\partial x_b} & \frac{\partial f_1(\mathbf{X})}{\partial y_b} & \frac{\partial f_1(\mathbf{X})}{\partial z_b} & \cdots & \frac{\partial f_1(\mathbf{X})}{\partial v_{s,x}} & \frac{\partial f_1(\mathbf{X})}{\partial v_{s,y}} & \frac{\partial f_1(\mathbf{X})}{\partial v_{s,z}} \\ \frac{\partial f_2(\mathbf{X})}{\partial x_b} & \frac{\partial f_2(\mathbf{X})}{\partial y_b} & \frac{\partial f_2(\mathbf{X})}{\partial z_b} & \cdots & \frac{\partial f_2(\mathbf{X})}{\partial v_{s,x}} & \frac{\partial f_2(\mathbf{X})}{\partial v_{s,y}} & \frac{\partial f_2(\mathbf{X})}{\partial v_{s,z}} \\ \vdots & \vdots & \vdots & \ddots & \vdots & \vdots & \vdots \\ \frac{\partial f_{12}(\mathbf{X})}{\partial x_b} & \frac{\partial f_{12}(\mathbf{X})}{\partial y_b} & \frac{\partial f_{12}(\mathbf{X})}{\partial z_b} & \cdots & \frac{\partial f_{12}(\mathbf{X})}{\partial v_{s,x}} & \frac{\partial f_{12}(\mathbf{X})}{\partial v_{s,y}} & \frac{\partial f_{12}(\mathbf{X})}{\partial v_{s,z}} \end{bmatrix} \tag{5}$$

For the filter is used a reduced form of Equations 1 and 2, considering only the gravitational forces referring to the Alpha and Beta bodies of the system:

$$\ddot{\mathbf{r}}_b = -\frac{\mu_{ab}}{r_b^3}\mathbf{r_b} \tag{6}$$

$$\ddot{\mathbf{r}}_s = -\frac{\mu_a}{r_s^3}\mathbf{r_s} + \mu_b\left[\frac{(\mathbf{r_b}-\mathbf{r_s})}{(r_b-r_s)^3} - \frac{\mathbf{r_b}}{r_b^3}\right] \tag{7}$$

For the model considered in this study, after the reduction of Equations 6 and 7 to the first order, the states are given by:

$$\mathbf{x} = \begin{bmatrix} x_b & y_b & z_b & v_{b,x} & v_{b,y} & v_{b,z} & x_s & y_s & z_s & v_{s,x} & v_{s,y} & v_{s,z} \end{bmatrix}^T \tag{8}$$

and Equation 3 is rewritten as follows:

$$\dot{\mathbf{x}} = \begin{bmatrix} f_1(\mathbf{x}) \\ f_2(\mathbf{x}) \\ f_3(\mathbf{x}) \\ f_4(\mathbf{x}) \\ f_5(\mathbf{x}) \\ f_6(\mathbf{x}) \\ f_7(\mathbf{x}) \\ f_8(\mathbf{x}) \\ f_9(\mathbf{x}) \\ f_{10}(\mathbf{x}) \\ f_{11}(\mathbf{x}) \\ f_{12}(\mathbf{x}) \end{bmatrix} = \begin{bmatrix} v_{b,x} \\ v_{b,y} \\ v_{b,z} \\ -\frac{\mu_{ab}}{r_b^3}\,x_b \\ -\frac{\mu_{ab}}{r_b^3}\,y_b \\ -\frac{\mu_{ab}}{r_b^3}\,z_b \\ v_{s,x} \\ v_{s,y} \\ v_{s,z} \\ -\frac{\mu_a}{r_s^3}\,x_s + \mu_b\left[\frac{(x_b-x_s)}{r_{bs}^3} - \frac{x_b}{r_b^3}\right] \\ -\frac{\mu_a}{r_s^3}\,y_s + \mu_b\left[\frac{(y_b-y_s)}{r_{bs}^3} - \frac{y_b}{r_b^3}\right] \\ -\frac{\mu_a}{r_s^3}\,z_s + \mu_b\left[\frac{(z_b-z_s)}{r_{bs}^3} - \frac{z_b}{r_b^3}\right] \end{bmatrix} \tag{9}$$

Therefore, the matrix F is given by:

$$\mathbf{F} = \begin{bmatrix} 0 & 0 & 0 & 1 & 0 & 0 & 0 & 0 & 0 & 0 & 0 & 0 \\ 0 & 0 & 0 & 0 & 1 & 0 & 0 & 0 & 0 & 0 & 0 & 0 \\ 0 & 0 & 0 & 0 & 0 & 1 & 0 & 0 & 0 & 0 & 0 & 0 \\ a_{31} & a_{33} & a_{33} & 0 & 0 & 0 & 0 & 0 & 0 & 0 & 0 & 0 \\ a_{41} & a_{42} & a_{43} & 0 & 0 & 0 & 0 & 0 & 0 & 0 & 0 & 0 \\ a_{51} & a_{52} & a_{53} & 0 & 0 & 0 & 0 & 0 & 0 & 0 & 0 & 0 \\ 0 & 0 & 0 & 0 & 0 & 0 & 0 & 0 & 0 & 1 & 0 & 0 \\ 0 & 0 & 0 & 0 & 0 & 0 & 0 & 0 & 0 & 0 & 1 & 0 \\ 0 & 0 & 0 & 0 & 0 & 0 & 0 & 0 & 0 & 0 & 0 & 1 \\ a_{101} & a_{102} & a_{103} & 0 & 0 & 0 & a_{107} & a_{108} & a_{109} & 0 & 0 & 0 \\ a_{111} & a_{112} & a_{113} & 0 & 0 & 0 & a_{117} & a_{118} & a_{119} & 0 & 0 & 0 \\ a_{121} & a_{122} & a_{123} & 0 & 0 & 0 & a_{127} & a_{128} & a_{129} & 0 & 0 & 0 \end{bmatrix} \tag{10}$$

the terms of the matrix are:

$$a_{31} = -\frac{\mu_{ab}}{r_{b,k-1}^3} + \frac{3\,\mu_{ab}\,\hat{x}_{b,k-1}^2}{r_{b,k-1}^5}$$

$$a_{32} = +\frac{3\,\mu_{ab}\,\hat{x}_{b,k-1}\,\hat{y}_{b,k-1}}{r_{b,k-1}^5}$$

$$a_{33} = +\frac{3\,\mu_{ab}\,\hat{x}_{b,k-1}\,\hat{z}_{b,k-1}}{r_{b,k-1}^5}$$

$$a_{41} = +\frac{3\,\mu_{ab}\,\hat{y}_{b,k-1}\,\hat{x}_{b,k-1}}{r_{b,k-1}^5}$$

$$a_{42} = -\frac{\mu_{ab}}{r_{b,k-1}^3} + \frac{3\,\mu_{ab}\,\hat{y}_{b,k-1}^2}{r_{b,k-1}^5}$$

$$a_{43} = +\frac{3\,\mu_{ab}\,\hat{y}_{b,k-1}\,\hat{z}_{b,k-1}}{r_{b,k-1}^5}$$

$$a_{51} = +\frac{3\,\mu_{ab}\,\hat{z}_{b,k-1}\,\hat{x}_{b,k-1}}{r_{b,k-1}^5}$$

$$a_{53} = +\frac{3\,\mu_{ab}\,\hat{z}_{b,k-1}\,\hat{y}_{b,k-1}}{r_{b,k-1}^5}$$

$$a_{53} = -\frac{\mu_{ab}}{r_{b,k-1}^3} + \frac{3\,\mu_{ab}\,\hat{z}_{b,k-1}^2}{r_{b,k-1}^5}$$

$$a_{101} = +\frac{\mu_b}{r^3_{bs,k-1}} + \frac{3\,\mu_b\,(\hat{x}_{b,k-1} - \hat{x}_{s,k-1})}{r^5_{bs,k-1}}\,(\hat{x}_{s,k-1} - \hat{x}_{b,k-1}) - \frac{\mu_b}{r^3_{b,k-1}} + \frac{3\,\mu_b\,\hat{x}^2_{b,k-1}}{r^5_{b,k-1}}$$

$$a_{102} = +\frac{3\,\mu_b\,(\hat{y}_{b,k-1} - \hat{y}_{s,k-1})}{r^5_{bs,k-1}}\,(\hat{x}_{s,k-1} - \hat{x}_{b,k-1}) + \frac{3\,\mu_b\,\hat{x}_{b,k-1}\,\hat{y}_{b,k-1}}{r^5_{b,k-1}}$$

$$a_{103} = -\frac{3\,\mu_b\,(\hat{z}_{b,k-1} - \hat{z}_{s,k-1})}{r^5_{bs,k-1}}\,(\hat{x}_{s,k-1} - \hat{x}_{b,k-1}) + \frac{3\,\mu_b\,\hat{x}_{b,k-1}\,\hat{z}_{b,k-1}}{r^5_{b,k-1}}$$

$$a_{107} = -\frac{\mu_b}{r^3_{bs,k-1}} + \frac{3\,\mu_b\,(\hat{x}_{b,k-1} - \hat{x}_{s,k-1})}{r^5_{bs,k-1}}\,(\hat{x}_{b,k-1} - \hat{x}_{s,k-1}) - \frac{\mu_a}{r^3_{s,k-1}} + \frac{3\,\mu_a\,\hat{x}^2_{s,k-1}}{r^5_{s,k-1}}$$

$$a_{108} = +\frac{3\,\mu_b\,(\hat{y}_{b,k-1} - \hat{y}_{s,k-1})}{r^5_{bs,k-1}}\,(\hat{x}_{b,k-1} - \hat{x}_{s,k-1}) + \frac{3\,\mu_a\,\hat{x}_{s,k-1}\,\hat{y}_{s,k-1}}{r^5_{s,k-1}}$$

$$a_{109} = +\frac{3\,\mu_b\,(\hat{z}_{b,k-1} - \hat{z}_{s,k-1})}{r^5_{bs,k-1}}\,(\hat{x}_{b,k-1} - \hat{x}_{s,k-1}) + \frac{3\,\mu_a\,\hat{x}_{s,k-1}\,\hat{z}_{s,k-1}}{r^5_{s,k-1}}$$

$$a_{111} = +\frac{3\,\mu_b\,(\hat{x}_{b,k-1} - \hat{x}_{s,k-1})}{r^5_{bs,k-1}}\,(\hat{y}_{s,k-1} - \hat{y}_{b,k-1}) + \frac{3\,\mu_b\,\hat{x}_{b,k-1}\,\hat{y}_{b,k-1}}{r^5_{b,k-1}}$$

$$a_{112,k-1} = +\frac{\mu_b}{r^3_{bs,k-1}} + \frac{3\,\mu_b\,(\hat{y}_{b,k-1} - \hat{y}_{s,k-1})}{r^5_{bs,k-1}}\,(\hat{y}_{s,k-1} - \hat{y}_{b,k-1}) - \frac{\mu_b}{r^3_{b,k-1}} + \frac{3\,\mu_b\,\hat{y}^2_{s,k-1}}{r^5_{b,k-1}}$$

$$a_{113} = +\frac{3\,\mu_b\,(\hat{z}_{b,k-1} - \hat{z}_{s,k-1})}{r^5_{bs,k-1}}\,(\hat{y}_{s,k-1} - \hat{y}_{b,k-1}) + \frac{3\,\mu_b\,\hat{y}_{b,k-1}\,\hat{z}_{b,k-1}}{r^5_{b,k-1}}$$

$$a_{117} = +\frac{3\,\mu_b\,(\hat{x}_{b,k-1} - \hat{x}_{s,k-1})}{r^5_{bs,k-1}}\,(\hat{y}_{b,k-1} - \hat{y}_{s,k-1}) + \frac{3\,\mu_a\,\hat{x}_{s,k-1}\,\hat{y}_{s,k-1}}{r^5_{s,k-1}}$$

$$a_{118} = -\frac{\mu_b}{r^3_{bs,k-1}} + \frac{3\,\mu_b\,(\hat{y}_{b,k-1} - \hat{y}_{s,k-1})}{r^5_{bs,k-1}}\,(\hat{y}_{b,k-1} - \hat{y}_{s,k-1}) - \frac{\mu_a}{r^3_{s,k-1}} + \frac{3\,\mu_a\,\hat{x}^2_{s,k-1}}{r^5_{s,k-1}}$$

$$a_{119} = +\frac{3\,\mu_b\,(\hat{z}_{b,k-1} - \hat{z}_{s,k-1})}{r^5_{bs,k-1}}\,(\hat{y}_{b,k-1} - \hat{y}_{s,k-1}) + \frac{3\,\mu_a\,\hat{y}_{s,k-1}\,\hat{z}_{s,k-1}}{r^5_{s,k-1}}$$

$$a_{121} = +\frac{3\,\mu_b\,(\hat{x}_{b,k-1} - \hat{x}_{s,k-1})}{r^5_{bs,k-1}}\,(\hat{z}_{s,k-1} - \hat{z}_{b,k-1}) + \frac{3\,\mu_b\,\hat{x}_{b,k-1}\,\hat{z}_{b,k-1}}{r^5_{b,k-1}}$$

$$a_{122} = +\frac{3\,\mu_b\,(\hat{y}_{b,k-1} - \hat{y}_{s,k-1})}{r^5_{bs,k-1}}\,(\hat{z}_{s,k-1} - \hat{z}_{b,k-1}) + \frac{3\,\mu_b\,\hat{x}_{b,k-1}\,\hat{z}_{b,k-1}}{r^5_{b,k-1}}$$

$$a_{123,k-1} = +\frac{\mu_b}{r^3_{bs,k-1}} + \frac{3\,\mu_b\,(\hat{z}_{b,k-1} - \hat{z}_{s,k-1})}{r^5_{bs,k-1}}\,(\hat{z}_{s,k-1} - \hat{z}_{b,k-1}) - \frac{\mu_b}{r^3_{b,k-1}} + \frac{3\,\mu_b\,\hat{z}^2_{b,k-1}}{r^5_{b,k-1}}$$

$$a_{127} = +\frac{3\,\mu_b\,(\hat{x}_{b,k-1} - \hat{x}_{s,k-1})}{r^5_{bs,k-1}}\,(\hat{z}_{b,k-1} - \hat{z}_{s,k-1}) + \frac{3\,\mu_a\,\hat{x}_{s,k-1}\,\hat{z}_{s,k-1}}{r^5_{s,k-1}}$$

$$a_{128} = +\frac{3\,\mu_b\,(\hat{y}_{b,k-1} - \hat{y}_{s,k-1})}{r^5_{bs,k-1}}\,(\hat{z}_{b,k-1} - \hat{z}_{s,k-1}) + \frac{3\,\mu_a\,\hat{y}_{s,k-1}\,\hat{z}_{s,k-1}}{r^5_{s,k-1}}$$

$$a_{129} = -\frac{\mu_b}{r^3_{bs,k-1}} + \frac{3\,\mu_b\,(\hat{z}_{b,k-1} - \hat{z}_{s,k-1})}{r^5_{bs,k-1}}\,(\hat{z}_{b,k-1} - \hat{z}_{s,k-1}) - \frac{\mu_a}{r^3_{s,k-1}} + \frac{3\,\mu_a\,\hat{z}^2_{s,k-1}}{r^5_{s,k-1}}$$

The Kalman filter consists of two phases, the propagation and updating phases. The propagation phase of time t_{k-1} to the next instant t_k is given as follows:

- The propagation of the state $\dot{\bar{\mathbf{x}}}$ will be done by integrating the equations of motion using the runge-kutta method in 7^a order, with initial condition $\bar{\mathbf{x}}_{k-1} = \hat{\mathbf{x}}_{k-1}$;
- The propagation of covariance will be done discreetly (Kuga, 2005):

$$\overline{\mathbf{P}}_k = \boldsymbol{\phi}_{k,k-1}\hat{\mathbf{P}}_{k-1}\boldsymbol{\phi}_{k,k-1}^t + \mathbf{Q}_k$$

where $\mathbf{Q}$ is the covariance of dynamic noise and $\phi_{k,k-1}$ is the transition matrix, given by:

$$\boldsymbol{\phi} = e^{\mathbf{F\Delta t}}$$

The phase of updating the filter by the measurements at the instant of time t_k is given by (Kuga, 2005):

$$\begin{aligned}
&\mathbf{K_k} = \bar{\mathbf{P}}_\mathbf{k}\mathbf{H}_\mathbf{k}^\mathbf{t}(\mathbf{H_k}\bar{\mathbf{P}}_\mathbf{k}\mathbf{H}_\mathbf{k}^\mathbf{t} + \mathbf{R_k})^{-\mathbf{1}} \\
&\hat{\mathbf{P}}_\mathbf{k} = (\mathbf{I} - \mathbf{K_k}\mathbf{H_k})\bar{\mathbf{P}}_\mathbf{k} \\
&\hat{\mathbf{x}}_\mathbf{k} = \bar{\mathbf{x}}_\mathbf{k} + \mathbf{K_k}(\mathbf{y_k} - \mathbf{H_k}\bar{\mathbf{x}}_\mathbf{k})
\end{aligned} \tag{11}$$

where $\mathbf{K_k}$ is the gain of Kalman, and $\hat{\mathbf{x}}_\mathbf{k}$ and $\hat{\mathbf{P}}_\mathbf{k}$ are the state and covariance updated to the instant k.

3. RESULTS

In this section the results of the study will be presented. The asteroid Didymos was chosen for the filter test. As mentioned earlier, this asteroid has a Moon (Didymoon, the Beta of the system) that orbits the main body (Didymos, the Alpha of the system). Table 1 shows the characteristics of Didymos-Didymoon system and the initial conditions for the simulations, the data were taken from HORYZONS system from NASA and Michel *et al.* (2016).

Tabela 1: Characteristics of the Didymos-Didymoon systems and initial conditions for the simulations.

Body	Didymos	Didymoon
Orbits	Sun	Didymos
Semi-major axis (a) [km]	246003643.42886	1.18
Eccentricity (e)	0.38375	0.03
Inclination (i) [degree]	3.4076	0.005
Orbital period	770.14 dias	11.92 horas
Equatorial radius [km]	0.39	0.0815
Mass [kg]	5.23×10^{11}	5×10^{9}
Obliquity [degree]	171	–
Argument of periapsis [degree]	319.25039	0
Longitude of ascending node [degree]	73.233299	0
Mean anomaly [degree]	96.832791	0

Through several tests to correctly regulate the filter for the Didymos-Didymoon system, in relation to estimating the trajectories of Didymoon and a spacecraft in orbit around Didymos, the values for $\mathbf{R}$ and $\mathbf{Q}$ were found:

$$\mathbf{Q} = 1 \times 10^{-6} * \mathbf{I}_{(12\times12)}$$

$$\mathbf{R} = \begin{bmatrix}(\sigma_1)^2 & (\sigma_1)^2 & (\sigma_1)^2 & (\sigma_2)^2 & (\sigma_2)^2 & (\sigma_2)^2 & (\sigma_1)^2 & (\sigma_1)^2 & (\sigma_1)^2 & (\sigma_2)^2 & (\sigma_2)^2 & (\sigma_2)^2\end{bmatrix} * \mathbf{I}_{(12\times12)}$$

where σ_1 is equal to 1×10^{-1} and σ_2 is equal to 1×10^{-3}. As previously mentioned, the measurement is provided linearly, with the positions and velocities coming directly from the complete model, but with an error introduced. This error is provided by using the matlab routine `randn` which generates a white noise. The generated values are multiplied by σ_1 for the positions and by σ_2 for the velocities. This is even if we introduce an error in the measures of ±100 meters for the positions and ±1 m/s for velocities, or at least approximately 68% of the measurement errors will be within these intervals, following the Gaussian distribution. In all simulations it was used as the initial covariance condition: $\overline{\mathbf{P}}_0 = \hat{\mathbf{P}}_0 = \mathbf{I}_{(12\times12)}$.

3.1 Estimation of trajectory of Didymoon

In this section we present the results for the estimation of position and velocity of Didymoon for a day, with updates occurring every 1 minute.

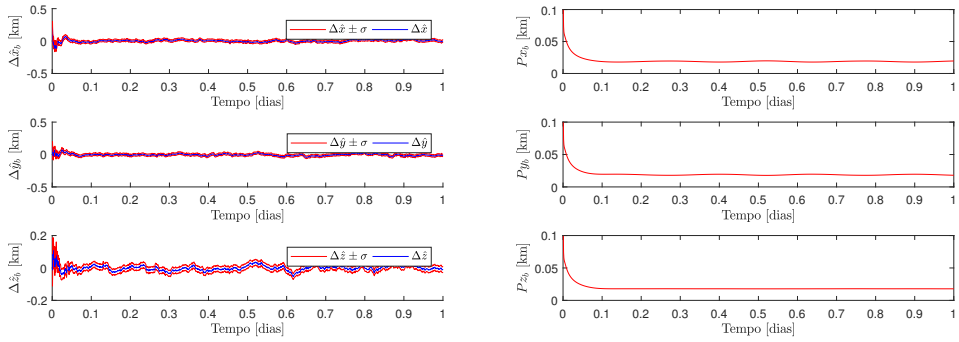

(a) (b)

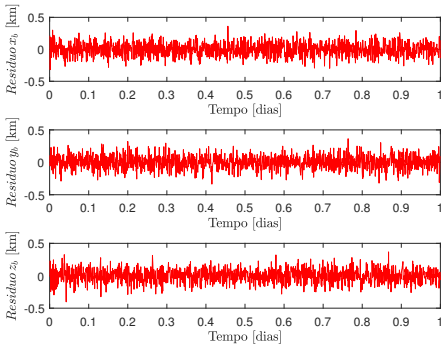

(c)

Figura 2: Results for the estimation of the position of Didymoon. (a) Error between the estimated position coordinates and that provided by the Didymoon reference model. (b) Standard deviation of the position coordinates estimated for Didymoon. (c) Residual estimates of position coordinates of Didymoon.

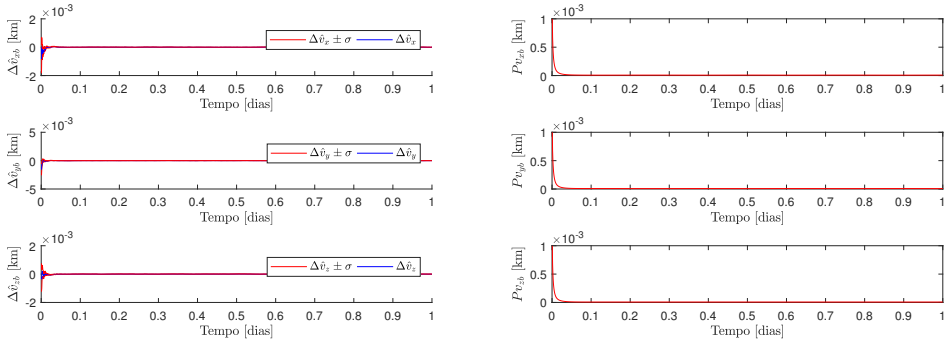

(a) (b)

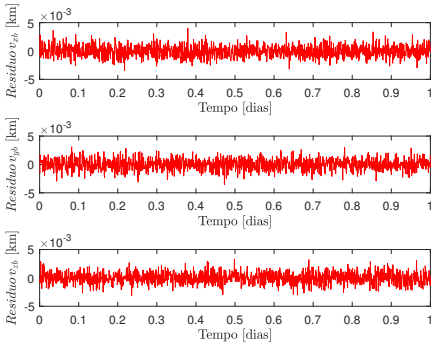

(c)

Figura 3: Results for the estimation of the speed of Didymoon. (a) Error between the estimated velocity coordinates and that provided by the Didymoon reference model. (b) Standard deviation of estimated velocity coordinates for Didymoon. (c) Residual estimates of Didymoon velocity coordinates.

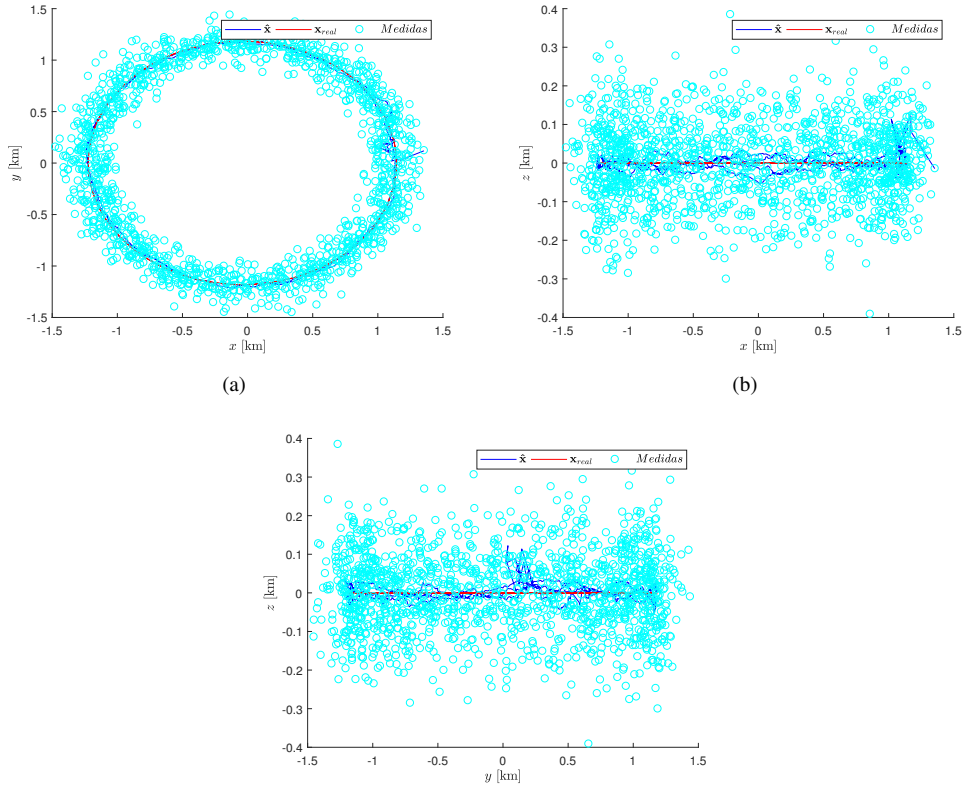

(a)

(b)

(c)

Figura 4: Estimated and reference trajectories of Didymoon. (a) View from the XY plane. (b) View from the XZ plane. (c) View from the YZ plane.

As shown in Figure 2(a), the filter was able to reduce the positioning error from 100 meters to less than 2 meters with a standard deviation of around 20 meters after the convergence of the filters, as shown in Figure 2(b). Another important behavior of the filter is showed in Figure 2(c), which shows that the residuals of the position estimates have an average close to zero, with a standard deviation of approximately ± 100 meters.

Analyzing Figure 3(a) we can note that the velocity error approached zero, going from the order of 10^{-3} to 10^{-6}. The same occurred for the standard deviation, as shown in Figure 3(b), which converged to near zero, being in the order of 10^{-5}. As shown in Figure 3(c), for the position the residue has mean zero, with standard deviation in the order of the noise introduced.

Figures 4(a), 4(b) e 4(c) show the dispersion of the measurements, the reference trajectories and the estimated ones. They give a real dimension of the problem, where even with a great dispersion of the measurements, the Kalman filter was able to put the reference or estimated orbits very close.

3.2 Estimation of the trajectory of a spacecraft in the Didymos-Didymoon system

Table 2 shows the initial conditions of the spacecraft, whether it was an orbit inside the orbit of Didymoon and with an eccentricity of 0.4, to force the spacecraft to pass near Didymoon.

Tabela 2: Initial conditions of the spacecraft.

Semi-major axis (a) [km]	0.79
Eccentricity (e)	0.4
Inclination (i) [degree]	0.005
Argument of periapsis [degree]	0
Longitude of ascending node [degree]	0
Mean anomaly [degree]	0

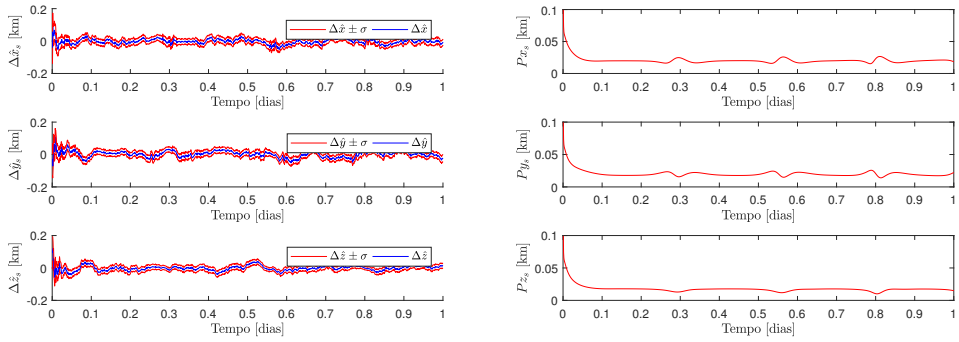

(a) (b)

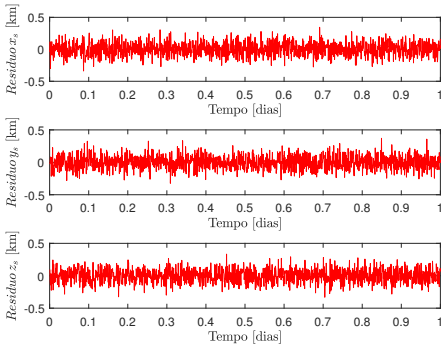

(c)

Figura 5: Results for the estimation of the position of the spacecraft. (a) Error between the estimated position coordinates and that provided by the spacecraft reference model. (b) Standard deviation of the estimated position coordinates for the spacecraft. (c) Residue of spacecraft position coordinates estimates.

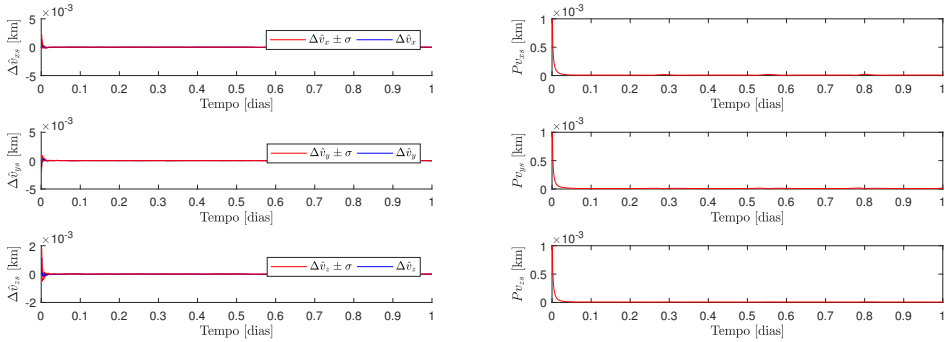

(a) (b)

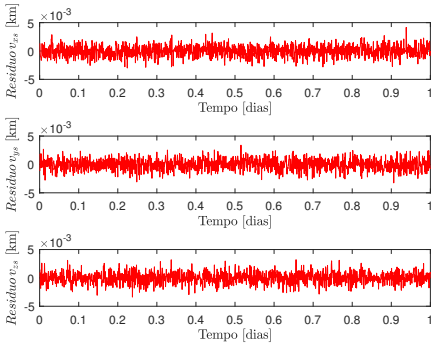

(c)

Figura 6: Results for the estimation of the velocity of the spacecraft. (a) Error between the estimated velocity coordinates and that given by the spacecraft reference model. (b) Standard deviation of the estimated velocity coordinates for the spacecraft (c) Residue of estimates of spacecraft velocity coordinates.

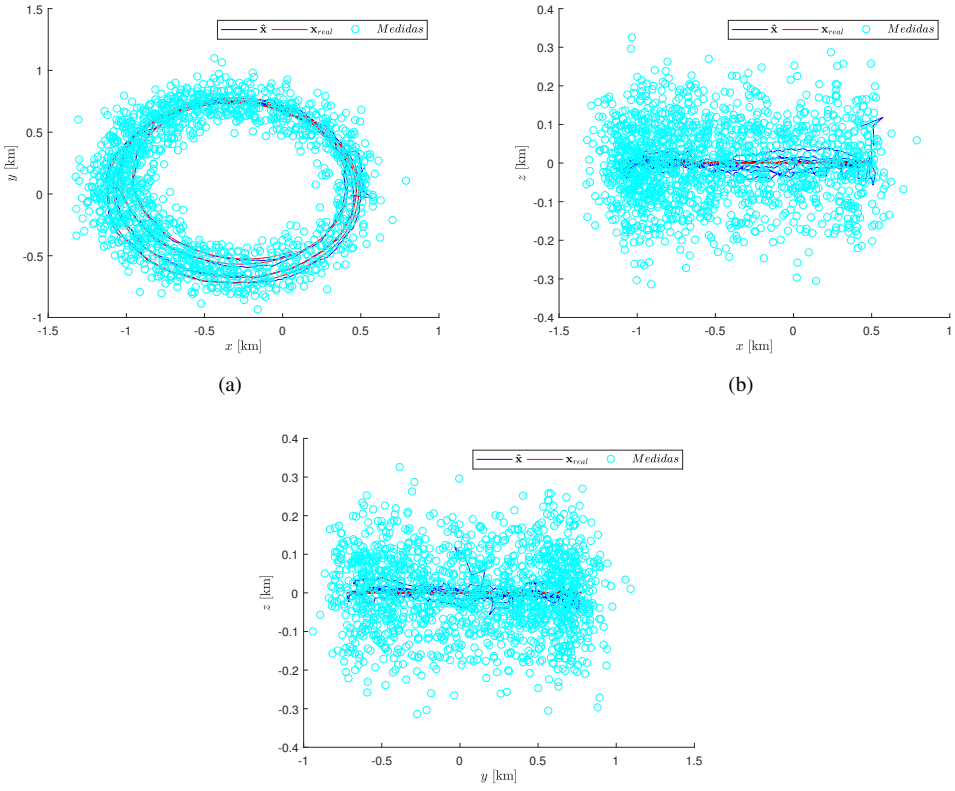

(a) (b)

(c)

Figura 7: Estimated and reference trajectories of the spacecraft. (a) View from the XY plane. (b) View from the XZ plane. (c) View from the YZ plane.

Figures 5(a) and 5(b) show that, as in the case for Didymoon, presented in Section 3.1, the position estimation error drops to 2 meters, with a standard deviation of 20 meters. What is striking are the three peaks of the standard deviation (Figure 5(b)), which probably occur in three close passages of the spacecraft by Didymoon. The filter does not diverge after these three moments. Figure 5(c) shows noise with mean zero and standard deviation close to the error of 100 meters.

Figures 6(a) and 6(b) show the estimation error and the standard deviation of the spacecraft velocity tending to zero, as in the case for Didymoon. In Figure 6(b), even if almost imperceptible, there are small peaks at the same instants of time as for the position estimate, indicating a spacecraft encounter with Didymos. Figure 6(c) shows that the residue has zero mean, with standard deviation in the order of the introduced error, as in Didymoon velocity estimation.

Figures 7(a), 7(b) and 7(c) show that, despite the great dispersion of measurements, even in this case where close encounters of the spacecraft with Didymoon occur, the extended Kalman filter was able to take the estimated path close to the reference path.

4. CONCLUSION

At the end of the study, the effectiveness of the Kalman extended filter is clear in minimizing the error from the sensor noise. Reducing position errors of the order of 100 meters for errors of 2 meters, with standard deviation of 20 meters and errors in the components of velocity of the order of 1 m/s tending to zero. The tuning of the filter was a great challenge because it was a dozen states. Future studies should consider the measures as non-linear, in order to approximate the results of the reality to be found.

5. ACKNOWLEDGMENT

The author thanks the grants # 406841/2016-0 and 301338/2016-7 from the National Council for Scientific and Technological Development (CNPq); and grants # 2014/22295-5, 2011/08171-3, 2016/14665-2 and 2016/07248-6 from São Paulo Research Foundation (FAPESP).

6. REFERENCES

Cui, W. and Zhu, K.J., 2014. "Comparison of three filters in asteroid-based autonomous navigation". *Research in Astronomy and Astrophysics*, Vol. 14, No. 3, p. 329.

Jagannathan, V., 1994. "Deep-space navigation - an overview". *IETE Technical Review*, Vol. 11, No. 4, pp. 197–204.

Kuga, H.K., 2005. *Notas de aula - Noções práticas de técnicas de estimção*. INPE.

Michel, P., Cheng, A., K, M., Pravec, P., Blum, J., Delbo, M., Green, S., Rosenblatt, P., Tsiganis, K., Vincent, J., Biele, J., Ciarletti, V., H9rique, A., Ulamec, S., Carnelli, I., Galvez, A., Benner, L., Naidu, S., Barnouin, O., Richardson, D., Rivkin, A., Scheirich, P., Moskovitz, N., Thirouin, A., Schwartz, S., Bagatin, A.C. and Yu, Y., 2016. "Science case for the asteroid impact mission (aim): A component of the asteroid impact & deflection assessment (aida) mission". *Advances in Space Research*, Vol. 57, No. 12, pp. 2529 – 2547. ISSN 0273-1177. doi:http://dx.doi.org/10.1016/j.asr.2016.03.031. URL http://www.sciencedirect.com/science/article/pii/S0273117716300692.

Rad, A.M. and Azari, L.V., 2014. "Determining attitude and position in deep space missions using x ray pulsars". *International Journal of Astronomy and Astrophysics*, Vol. 4, No. 04, p. 628.

Riedel, J., Bhaskaran, S., Desai, S., Hand, D., Kennedy, B., McElrath, T. and Ryne, M., 2000. "Autonomous optical navigation(autonav) ds 1 technology validation report". *Deep Space 1 technology validation reports(A 01-26126 06-12), Pasadena, CA, Jet Propulsion Laboratory(JPL Publication 00-10), 2000*.

Wood, L., Bhaskaran, S., Border, J., Byrnes, D., Cangahuala, L., Ely, T., Folkner, W., Naudet, C., Owen, W., Riedel, J. *et al.*, 2012. "Guidance, navigation, and control technology assessment for future planetary science missions, part 1: Onboard and ground navigation and mission design". Technical report, Technical report, Strategic Missions and Advanced Concepts Office, NASA JPL.

7. RESPONSABILIDADE AUTORAIS

Os autores são os únicos responsáveis pelo conteúdo deste trabalho.